The Point of no Return in Climate Change

BRENDA C. VAN ZALINGE, HENK A. DIJKSTRA

Institute for Marine and Atmospheric Research Utrecht, Utrecht University, Utrecht, the Netherlands

ABSTRACT

The Global Mean Surface Temperature (GMST) has been increasing as a result of anthropogenic emission of green house gasses (GHGs), since the industrial revolution. If we continue to emit equal amounts of GHGs as we do today, then Earth's climate will suffer irreversible changes by the end of this century. Therefore, it is crucial that the anthropogenic emission of GHGs is regulated and significantly reduced before such irreversible impacts occur. However, there is no good quantitative measure for when exactly these irreversible impacts will occur and hence it is extremely challenging to determine when it is "too late" to start reducing GHGs. The point in time at which it will be "too late" to reduce GHGs is indicated by the point of no return. In this study, we define and subsequently search for the point of no return in climate change using stochastic viability theory. Thereafter we investigate when and how much the GHGs concentration should be reduced, using an economical approach. A cost function is defined, which gives the economic costs for a certain CO_2eq reduction scenario. We then apply this novel approach to two climate models, including PLASIM. Using linear response theory in combination with data from PLASIM, we find that major reductions in the CO_2eq concentration should occur before 2065 to guarantee that the GMST is not more than 2 °C higher than the preindustrial GMST in 2100. Furthermore, we found an optimal CO_2eq reduction scenario, that minimises the economic costs. We consider that the novel approach presented in this study is a strong decision-making tool during future debates about climate change.

1 Introduction

The concentration of greenhouse gases (GHGs) in the atmosphere has been increasing since the industrial revolution. This increase is caused by anthropogenic emission of GHGs and is associated with a rise in global mean surface temperature (GMST). In the last Synthesis Report of the Intergovernmental Panel of Climate Change (IPCC), Pachauri et al. (2014a) stated with high confidence: "Without additional mitigation efforts beyond those in place today, and even with adaptation, warming by the end of the 21st century will lead to high to very high risk of severe, widespread and irreversible impacts globally". Such irreversible global impacts include the shutdown of the Atlantic thermohaline circulation and the collapse of the Greenland and Antarctic ice sheet (Lenton et al. 2008). If no measures are taken to reduce GHG emission during this century and neither will there be any new technological developments that can reduce GHGs in the atmosphere, it is likely that the GMST will be 4 °C higher than the preindustrial GMST at the end of the 21st century (Pachauri et al. 2014a). Under this temperature change, the Greenland ice sheet will collapse and the sea level will rise between the 2 and 7 meters (Lenton et al. 2008). Consequently, it is important that anthropogenic emission is regulated and significantly reduced before widespread and irreversible impacts occur. This is, however, extremely challenging, as there is no good quantitative measure for when it is "too late" and thus when irreversible global impacts will take place.

The moment at which it is "too late" to take action is often called the point of no return. A few studies have tried to define this point of no return. Firstly, Hansen et al. (2008) defined the point of no return as a certain CO_2 concentration and concluded that if humanity desires to life on a planet similar to which we have adapted over the last 12000 years, then the CO_2 concentration will need to be reduced to 350 ppmv. This definition, however, assumes that the present climate is only forced by the CO_2 concentration, while in reality other GHGs play a crucial role in increasing the GMST as well. Secondly, Rogelj et al. (2013) defined the point of no return as a certain GHG emission level in 2020. The authors proposed that the point of no return is reached when the GHG emission level in 2020 guarantees there is a "high-probability" that the GMST will become 2 °C higher than the preindustrial GMST. However, the authors are not specific about what they mean with a "high probability", and thus there is need to better understand the point of no return in climate change.

In this study, we aim to define the point of no return more precisely using the stochastic viability theory. We

define the point of no return as a point in time before we need to significantly reduce the GHG concentrations. In contrast to the study by Hansen et al. (2008) we consider all GHGs that force the present-day climate. Specifically, we express the combined GHGs as the CO2 equivalence concentration (CO_2eq), which has the same global warming potential as the GHGs combined.

In the second part of this study, we investigate when and how much the GHG concentration should be reduced using an economical approach. A lot of research has been done on the economics of climate change (Nordhaus 1994; Tol 2002; Stern 2007), but we are the first that combine this with the point of no return. We design a cost function, which gives the economic cost expressed in US dollars for a certain CO_2eq reduction scenario. Such a CO_2eq reduction scenario is called a mitigation scenario throughout this study. The aim is to find a optimal mitigation scenario, which is the scenario with the lowest economic costs. This approach is applied using two different climate models. The first model is a simple energy balance model, which we use to illustrate the influence of a tipping point on the point of no return and the optimal mitigation scenario. Although this first model is highly simplified, it provides an insight in the concept of the point of no return, which is the foundation of this work. Subsequently, we use data from the Planet Simulator (PLASIM) (Ragone et al. 2014), which is a climate model of intermediate complexity (Fraedrich et al. 2005), in combination with linear response theory, to find the point of no return and the optimal mitigation scenario. We evaluate the results of the models separately. This implies that we first discuss the results of the energy balance model, before introducing PLASIM.

This study provides new insights in how to define a point of no return in climate change. We furthermore indicate that major reduction in CO_2eq concentration should occur before 2065 to guarantee that the GMST is not more than 2 °C higher than the preindustrial GMST in 2100. Furthermore, we consider the novel approach presented in this study as a strong decision-making tool during future debates about climate change.

2 Methodology

In this section we introduce the general theories and concepts used in this study. Firstly, stochastic viability theory is explained and stochastic viability kernels are introduced. Secondly, we define the point of no return. Subsequently, we explain at which point in time, before the point of no return, we aim to reduce the CO_2eq concentration. This we call the time of action. We then introduce the economic cost function for a certain mitigation scenario. Finally, linear response theory is explained, which will be used in order to find the point of no return in PLASIM.

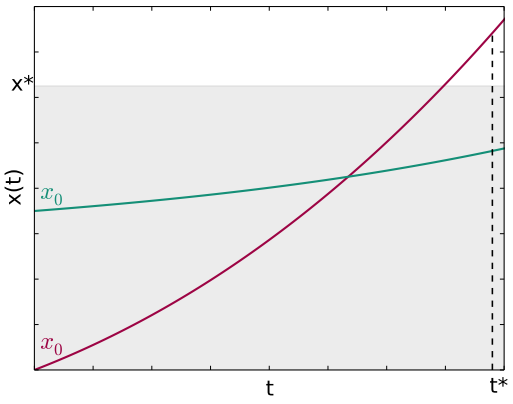

FIG. 1: An example of a viable and non viable initial condition in deterministic viability theory for a certain dynamical system given by $x'(t) = F(x(t))$. The red and green line represent the time evolution of x. The considered viable region V is given by $x \leq x^*$ and is indicated by the grey area. According to expression 1, initial condition x_0 is viable and x_0 non viable.

2.1 *Stochastic viability theory*

To define a point of no return in climate change, we use viability theory. This theory studies the evolution of dynamical systems under constraints on the system's state (Aubin 2009). These constraints define a region V, which is considered as the viable region. Assume a dynamical system $x'(t) = F(x(t))$ and a initial condition $x(0) = x_0 \in V$. In the deterministic viability theory, the initial condition x_0 is called viable if

$$\text{for } t \leq t^* : x(t) \in V, \tag{1}$$

with t^* being a certain end time. In Fig. 1, an example of a viable and non viable initial condition are given in a situation where the viable region V is given by $x \leq x^*$. Finally, a viability kernel can be created, which consists of all viable initial conditions x_0.

As the climate system is stochastic rather than deterministic, stochastic viability theory must be used. Suppose X_t is a stochastic variable that has a certain normalised probability density function (PDF) $p(x,t)$ and assume a discrete stochastic dynamical system given by $X_{t+1} = F(X_t)$ with initial condition X_0. In order to say anything about the viability of X_0, stochastic viability kernels (V_β) were introduced (Doyen and De Lara 2010). A stochastic viability kernel V_β consists of initial conditions X_0 for which the system has, for $t \leq t^*$, a probability β or higher to stay in viable region V. When the viable region V is given by

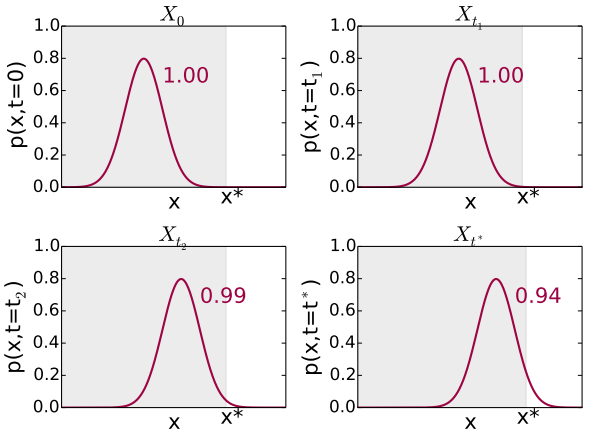

FIG. 2: An example of an initial condition that is in $V_{0.94}$. The considered viable region V is given by $x \leq x^*$ and is indicated by the grey area. For X_0, X_{t_1}, X_{t_2} and X_{t^*}, with $0 < t_1 < t_2 < t^*$, the associated PDF is plotted. The hypothetical system F shifts the PDF gradually to the right over time. The number indicated in the plots corresponds to result of integral $\int_0^{x^*} p(x,t)\,dx$.

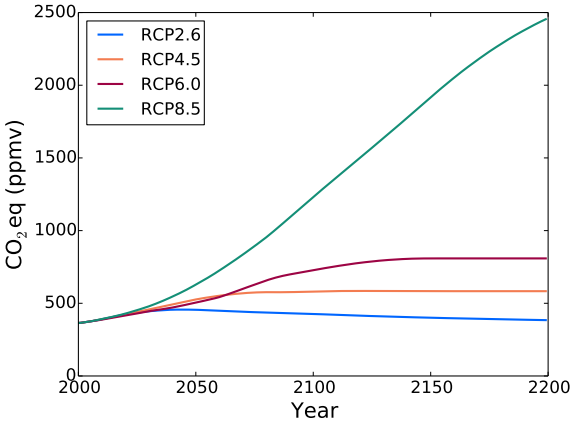

FIG. 3: GHG trajectories used by the IPCC. These CO_2eq scenarios are possible climate futures.

$x \leq x^*$, this is symbolically given by

$$X_0 \in V_\beta \qquad \text{if} \qquad \text{for } t \leq t^* : \int_0^{x^*} p(x,t)\,dx \geq \beta. \quad (2)$$

An example of an initial condition X_0 that is in $V_{0.94}$ is given in Fig. 2. Note that if $X_0 \in V_{0.94}$, then also $X_0 \in V_\beta$ with $\beta < 0.94$.

Apart from calling an initial condition X_0 viable, X_t can be called viable as well. When introducing a tolerance probability β_T, the stochastic variable X_t is called viable if

$$\int_0^{x^*} p(x,t)\,dx \geq \beta_T. \quad (3)$$

When the integral is less than β_T, X_t is called non viable.

2.2 *Point of no return*

The aim of this subsection is to define the point of no return of a climate system forced by a Representative Concentration Pathway (RCP) scenario. RCP scenarios are GHG trajectories used by the IPCC. There are four RCP scenarios (shown in Fig. 3) and they are all possible climate futures (Pachauri et al. 2014a). Before defining the point of no return, a collection F must be introduced, which consists of possible mitigation scenarios. For instance, F could consist of mitigation scenarios that exponentially decay to different CO_2eq stabilisation levels within a certain time. An example of the collection F is shown in Fig. 4, in which the mitigation scenarios are indicated by the dashed and dotted red lines. The most extreme scenario from F is defined as the mitigation scenario which has the steepest initial gradient (dashed line in Fig. 4). Assume now a discrete stochastic climate system which is forced by a RCP scenario. The considered stochastic variable in this climate system is X_t. Finally, we have made two different definitions for the point of no return: for a given RCP scenario, tolerance probability β_T, viable region V and collection F, the point of no return (π_t) is defined as the first year where, even when at that moment the most extreme mitigation scenario from F is applied,

- X_t will be non viable for more than T_T years, where T_T is a set tolerance time.
- X_t will be non viable in 2100.

The first definition is based on limiting the amount of years that X_t is non viable, since during these years we are exposed to risks from, for example, extreme weather events. The second definition imposes no restrictions on how long X_t can be non viable, however, it guarantees that X_t is viable at the end on the century. This is definition is based on the fact that climate change must be limited at the end of the century (Pachauri et al. 2014a). Furthermore, note that the definition of the point of no return can easily be changed according to any desired political policy.

The first and second definition will be used to find the point of no return in the energy balance model and PLASIM, respectively.

2.3 *Time of action*

Once the point of no return for a given RCP scenario is known, the aim is to avoid this point in time and start mitigating the CO_2eq concentration before π_t. The moment

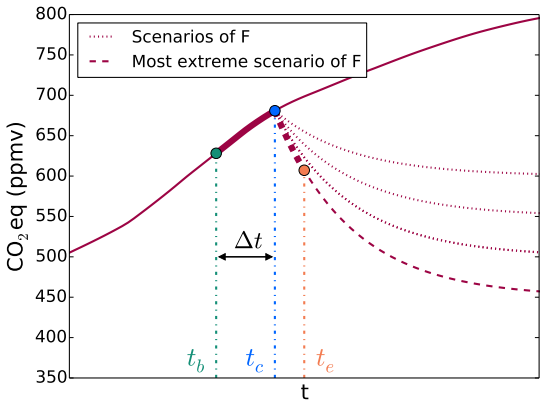

FIG. 4: An overview of the introduced parameters. The solid red line represents a RCP scenario. At each time we can calculate X_t with the climate model and subsequently check whether it is viable or not. When the mitigation is according to the most extreme scenario of F, the period at which X_t is non viable is indicated by the bold part of the solid and dashed line (between t_b and t_e).

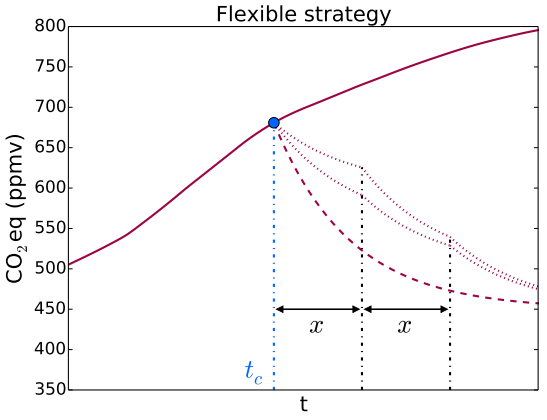

FIG. 5: An illustration on how the flexible mitigation strategy works. Every x years the scenario from F with which is mitigated can be re-chosen. The two dotted lines are examples of possible scenarios of the flexible strategy at which we re-choose the scenario from F every x years. The dashed line indicates a scenario at which every x years is chosen to mitigate further with the same scenario from F as is already used.

at which the CO_2eq mitigation scenario is applied, we call the time of action and is indicated by t_c.

When forcing the climate system with a RCP scenario, at a certain time X_t may not be viable anymore. The first year of non viability of X_t is indicated by t_b. Once X_t is not viable, ideally we want to control the CO_2eq concentration directly such that X_t will become viable again. However, since reducing CO_2eq emission is accompanied with technological, social, economic and institutional challenge, the mitigation will be delayed (Pachauri et al. 2014a). Therefore, in this study we assume that the time of action is Δt years after the first year of non viability. This means that $t_c = t_b + \Delta t$. From the time of action, the CO_2eq concentration will decrease according to one of the mitigation scenarios in F. Eventually, X_t will become viable again and this point in time is indicated by t_e. An overview of the introduced parameters can be found in Fig. 4.

2.4 *Mitigation strategies*

The mitigation strategy that is discussed above and shown in Fig. 4 is called the fixed strategy. This strategy implies that at $t = t_c$ a scenario from F is chosen and subsequently for $t \geq t_c$ the CO_2eq concentration is given by that scenario. These scenarios will be collected in a new collection F_{fix}. However, we also consider a flexible mitigation strategy. This implies that every x years the scenario with which is mitigated can be re-chosen. For example, at $t = t_c$, we decide to mitigate with a scenario from F that stabilises at a rather high CO_2eq concentration. However, at $t = t_c + x$, we notice that the mitigation is going to slow and decide to mitigate with a scenario that stabilises at a lower CO_2eq concentration (see Fig. 5). The way in which the scenario at $t = t_c + x$ is chosen can be based on the PDF of X_{t_c+x} or randomly. All the possible mitigation scenarios that can be made using the flexible strategy are gathered in the collection F_{flex}.

2.5 *Cost function*

Once we know when to reduce the GHG concentration, we can determine the most optimal way to reduce the CO2eq concentration. We will investigate this from an economical point of view. The goal is to find the optimal mitigation scenario which is defined as the mitigation scenario for which the economic costs are minimised. To find the optimal mitigation scenario, a cost function Ψ is introduced that gives the economic costs for a certain mitigation scenario. Symbolically, the optimal mitigation scenario, using the fixed mitigation strategy, is given by

$$f^*(t) = \min_{f(t)\in F_{fix}} \{\Psi\big(f(t)\big)\}. \tag{4}$$

To find the optimal mitigation scenario using the flexible strategy, F_{fix} should be substituted by F_{flex} in Eq. 4.

Modelling the economic costs that are made as a result of climate change and mitigation on a global scale is very complex. One must consider an extensive range of

economic, social and environmental issues (Stern 2007). There are several studies that have modelled the economic costs of climate change, including Nordhaus (1994) and Tol (2002). However, we do not have access to these models. Therefore, we design our own cost function.

The goal of this study is to design an acceptable cost function Ψ to demonstrate the concept of steering the CO_2eq concentration, such that X_t becomes viable again, by minimising the economic costs, rather than to design the most realistic economic cost function. Therefore, our cost function Ψ will only consider costs associated with stringency of mitigation and damage from extreme weather events, which include heatwaves, flooding and hurricanes. A cost function which only includes these expenses is suitable to find the optimal mitigation scenario. Other costs of climate change, which are thus not considered, include costs associated with sea level rise, agriculture and human health.

The explicit cost function used to make the results for the energy balance model and PLASIM are different and can be found later in this paper.

2.6 Linear response theory

In order to find the temporal evolution of the PDF of X_t under any CO_2eq forcing in PLASIM, we will use response theory. With response theory, the effect of any small forcing perturbation on the system state can be calculated by running the climate model for only one forcing scenario.

To find the temporal evolution of the PDF of X_t, we assume that the PDF of X_t is Gaussian. Consequently, once the temporal evolution of the expectation value and variance of X_t ($E[X_t]$ and $VAR[X_t]$) are found, the PDF of X_t is known. In order to find this temporal evolution for any CO_2eq forcing, we will use the linear response theory, and therefore the so-called Green functions of the expectation value and variance must be found. We want to derive the first order Green function of these observables, which accounts for the linear response of the full nonlinear climate system.

To derive the first order Green functions, Ruelle's response theory (RRT) is used, which is a general method to study the response of nonequilibrium systems to external perturbations (Ruelle 1998, 2009). Ragone et al. (2014) have argued that RRT is applicable to the statistical properties of a climate model. Also, they have shown that RRT extends to rather intense finite perturbations in the forcing instead of infinitesimal perturbations.

Ruelle illustrated that the expectation value of an observable Φ, when forcing the system with $f(t)$, can be calculated as a perturbative expansion following the formula:

$$\langle \Phi \rangle_f(t) = \langle \Phi \rangle_0 + \sum_{n=1}^{+\infty} \langle \Phi \rangle_f^{(n)}(t). \tag{5}$$

In this formula, $\langle \Phi \rangle_0$ is the expectation value of observable Φ in the unperturbed state and $\langle \Phi \rangle_f^{(n)}(t)$ are the perturbative terms. The linear response of the system is given by $\langle \Phi \rangle_f^{(1)}(t)$ and can be found by computing the convolution of the first order Green function $G^{(1)}_{\langle \Phi \rangle}$ and forcing $f(t)$, which is given by

$$\langle \Phi \rangle_f^{(1)}(t) = \int_{-\infty}^{+\infty} G^{(1)}_{\langle \Phi \rangle}(\tau) f(t-\tau) d\tau. \tag{6}$$

Therefore, once the first order Green function is known, the linear response can be calculated, for any forcing $f(t)$.

To construct the linear Green function, it is used that the convolution in the time domain is the same as pointwise multiplication in the frequency domain. Hence, the Fourier transform of Eq. 6 is given by

$$\widetilde{\langle \Phi \rangle}_f^{(1)}(\omega) = \chi^{(1)}_{\langle \Phi \rangle}(\omega) \widetilde{f}(\omega), \tag{7}$$

with $\chi^{(1)}_{\langle \Phi \rangle}(\omega)$, $\widetilde{\langle \Phi \rangle}_f^{(1)}(\omega)$ and $\widetilde{f}(\omega)$ being the Fourier transforms of $G^{(1)}_{\langle \Phi \rangle}(t)$, $\langle \Phi \rangle_f^{(1)}(t)$ and $f(t)$, respectively. Therefore, once the time evolution of the expectation value of an observable under a certain forcing is known, the linear Green function of this observable can be constructed with Eq. 7 and consequently the linear response for any forcing can be calculated. Since Ragone et al. (2014) have argued that RRT is applicable to statistical properties of a climate model, the same principle is used to calculate the variance of observable Φ.

3 Energy balance model

The idealised energy balance model that we will use is of Budyko-Seller type (Budyko 1969; Sellers 1969) as formulated in Hogg (2008) and given by

$$c_T \frac{dT}{dt} = \underbrace{Q_0(1-\alpha(T))}_{1} + \underbrace{G + A \ln \frac{C(t)}{C_0}}_{2} - \underbrace{\sigma \varepsilon T^4}_{3}. \tag{8}$$

In this equation, term 1 represents the short-wave radiation received by the surface. In this first term, $\alpha(T)$ is the albedo, which depends on temperature. The albedo function is given by

$$\begin{aligned} \alpha(T) = \alpha_0 H(T_0 - T) + \alpha_1 H(T - T_1) + \\ \big(\alpha_0 + (\alpha_1 - \alpha_0)\frac{T - T_0}{T_1 - T_0}\big) H(T - T_0) H(T_1 - T). \end{aligned} \tag{9}$$

This equation contains the effect of land ice on the energy balance and $H(x) = (1 + \tanh(x/\varepsilon_H))/2$ is a continuous approximation of the Heaviside function. When the temperature $T < T_0$, the albedo will be α_0 and when

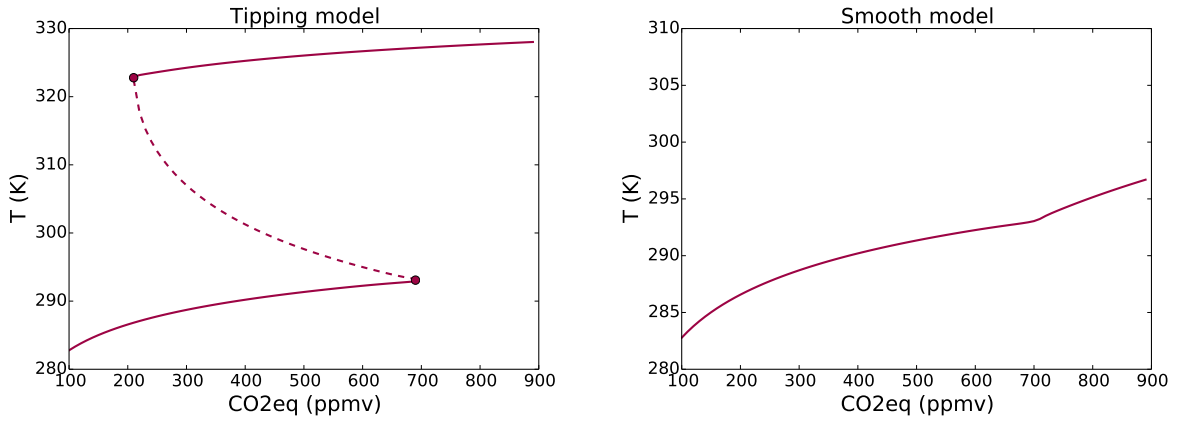

(a) (b)

FIG. 6: Bifurcation diagram for $\alpha_1 = 0.2$ ((a), tipping model) and $\alpha_1 = 0.45$ ((b), smooth model). The solid line represents a stable equilibrium while a dashed line represents an unstable equilibrium. The lower stable branch of the tipping model coincide with the smooth model. Note the difference in scale on the vertical axis for both plots.

$T > T_1$ it will be α_1. Furthermore, if $T_0 \leq T \leq T_1$, a linear relation for the albedo is assumed.

Term 2 represents the effect of greenhouse gases on the energy balance. It consists of a constant part, G, and a part which value is determined by the global mean CO_2eq concentration in the atmosphere ($C(t)$). Finally, term 3 in Eq. 8 expresses the effect of long-wave radiation on the energy balance. The variable T is the GMST which is given in Kelvin. The values and meaning of the parameters in Eq. 8, if not discussed in the text, are given in Table 1.

3.1 *Constant CO_2eq case*

When using C in Eq. 8 as a time-independent control parameter, a bifurcation diagram can be made in which the global mean CO_2eq concentration is plotted versus the equilibrium GMST. As shown in Table 1, we consider two different values for α_1. The bifurcation diagram corresponding to $\alpha_1 = 0.2$ has a tipping point which is absent when using $\alpha_1 = 0.45$. Both original bifurcations are shifted with 30 K upward such that we get the bifurcations seen in Fig. 6. This is done such that all concepts can be demonstrated rather than having the most realistic output. Throughout the rest of this study we will use this "shifted" model. Also, from now on, the energy balance model with $\alpha_1 = 0.2$ and $\alpha_1 = 0.45$ will be called tipping model and smooth model, respectively.

3.2 *Stochastic case*

If we suppose the effect of small scale processes on the energy balance is represented by noise, the energy balance model is given by Itô stochastic differential equation

TABLE 1: Value and meaning of the parameters in the energy balance model given by Eq. 8.

Parameter	Value	Meaning
c_T	5.0 x 10^8 $Jm^{-2}K^{-1}$	Thermal inertia
ε	1.0	Emissivity
Q_0	342 Wm^{-2}	Solar constant divided by four
σ	5.67 x 10^{-8} $Wm^{-2}K^{-4}$	Stefan Boltzmann constant
A	2.05 x 10^1 Wm^{-2}	Controls the equilibrium climate sensitivity
C_0	280 ppmv	Reference CO_2 concentration
G	1.5 x 10^2 Wm^{-2}	
α_1	0.2 or 0.45	
α_0	0.7	
T_1	293 K	
T_0	263 K	
ε_H	0.273 K	

shown by

$$dX_t = \frac{1}{c_T}\Big\{Q_0(1-\alpha(X_t)) + G + A\ln\frac{C(t)}{C_0} - \sigma\varepsilon {X_t}^4\Big\}dt + \sigma_s dW_t. \qquad (10)$$

In this equation, X_t is the stochastic GMST and σ_s is the typical standard deviation of the noise. We have chosen σ_s such that the variance of the noise (${\sigma_s}^2$) is three per cent of the value of $\frac{G}{c_T}$. This is an unrealistically high value. However, when choosing the variance of the noise more realistically, the PDF of the temperature will almost be a delta function and hence concepts cannot be demonstrated.

Since X_t is a stochastic variable it is characterised by a certain normalised PDF $p(x,t)$. This PDF will change over time when the CO_2eq concentration in the atmosphere is varying. Because Eq. 10 is an Itô process, $p(x,t)$ is given according to the Fokker-Planck equation. Before applying the Fokker-Planck equation, we will rewrite the Eq. 10 as

$$dX_t = f(X_t,t)dt + \sigma_s dW_t, \tag{11}$$

with $f(X_t,t) = \frac{1}{c_T}\{Q_0(1-\alpha(X_t)) + G + A\ln\frac{C(t)}{C_0} - \sigma\varepsilon {X_t}^4\}$. The Fokker-Planck equation of the stochastic energy balance model is given by

$$\frac{\partial p}{\partial t} + \frac{\partial (fp)}{\partial x} - \frac{\sigma_s^2}{2}\frac{\partial^2 p}{\partial x^2} = 0. \tag{12}$$

This differential equation can be solved numerically for $p(x,t)$ under any CO_2eq forcing when having two boundary conditions ($p(x_u,t) = p(x_l,t) = 0$) and an initial condition ($\int_{x_l}^{x_u} p(x,0)dx = 1$).

3.3 Mitigation scenarios

In this stage of the study, the collection F consists of mitigation scenarios that exponentially decay to the preindustrial CO_2eq concentration, which is 280 ppmv. For this exponential decay, we consider different e-folding times, which is indicated by the symbol k. As most extreme mitigation scenario an exponential decay within 50 years is considered, which corresponds to e-folding time of $k = 9$ years. Finally, the collection F consist of mitigation scenarios for which $k \geq 9$. Symbolically, a mitigation scenario with an e-folding time of k years is given by

$$f_k(t) = \big(\mathrm{CO_2eq}|_{t_{st}} - 280\big)\exp\Big(-\frac{t-t_{st}}{k}\Big) + 280. \tag{13}$$

In this equation is t_{st} the time at which the mitigation scenario is applied and $\mathrm{CO_2eq}|_{t_{st}}$ the associated CO_2eq concentration at that moment. The collection F_{fix}, which is the collection used to find the optimal mitigation scenario using the fixed strategy, is filled with the scenarios of F with $t_{st} = t_c$.

To find the optimal mitigation scenario using the flexible strategy, we need to create the collection F_{flex}. In this stage of the study, the scenarios in F_{flex} are made by rechoosing your mitigation scenario from F every 5 years. The way in which this choice is made, is based on the expectation value of the GMST at the moment of reconsidering. The higher $E[X_t]$, the faster we want to mitigate, the smaller the e-folding time. We will consider several linear relationships between k and $E[X_t]$. This relationship gives an answer on how the scenario from F at the moment of reconsidering should be selected. Each linear relation will create a scenario in F_{flex}. Finally, we calculate which scenario in F_{flex} minimises the economic costs, or in other words which linear relation between k and $E[X_t]$ minimises the economic costs.

Since there are infinitely many linear relationships between k and $E[X_t]$, a reference expectation value $E^*[X_t]$ and e-folding time k^* are introduced. These values are used in such a way that when the expectation value has a value of $E^*[X_t]$, the scenario that will be chosen from F is always the scenario with e-folding time k^*. We choose $E^*[X_t]$ as the value of the expectation value of the GMST just before getting non viable and the associated k^* is set at 200 years.

$$k = 200 + \gamma(E[X_t] - E^*[X_t]) \tag{14}$$

Finally, the linear relationship between k and $E[X_t]$ is given by Eq. 14. We will consider different values for γ and calculate for which γ the economic costs are minimised.

3.4 Cost function

The cost function used to find the optimal mitigation scenario in the energy balance model is simple. The part of the cost function which considers costs associated with the stringency of mitigation is based on the statement that (with high confidence) costs of mitigation increase with the stringency of mitigation (Pachauri et al. 2014b). We assign costs for mitigation between the time we start mitigating (t_c) and the time that X_t will be viable again (t_e). To do this, the surface between the CO_2eq scenario and a reference CO_2eq level (C_{ref}) is used. When the mitigation is more stringent, this surface will be smaller. Consequently, the costs are given by the inverse of the surface.

$$\Psi\big(f(t)\big) = \underbrace{\zeta\Big(\int_{t_c}^{t_e}\big(f(t) - C_{ref}\big)dt\Big)^{-1}}_{1} + \underbrace{(t_e - t_b)^2}_{2} \tag{15}$$

In Eq. 15, this part of the cost function is given by 1, where ζ is a weighting factor to scale with the costs given in part 2 and $f(t)$ is the mitigation scenario. The costs are given in 10^{12} US$.

The second part of the cost function is related to time that the GMST has not been viable. When the GMST is not viable, the temperature distribution exceeds a threshold. The longer the GMST stays non-viable, the longer we are exposed to risks from extreme events such as heat waves, heavy precipitation and coastal flooding (Pachauri et al. 2014b). Such events will be accompanied with damage to nature and buildings. The recovery costs of this is modelled in part 2 of Eq. 15 by a quadratic relation. Finally, the optimal mitigation scenario can be determined for the fixed and flexible strategy by minimising Eq. 15 under the constraint that $t_e - t_b \leq T_T$, where T_T is a set tolerance time.

4 Results energy balance model

In this section, we present the results generated with the idealised energy balance model. Firstly, we show which future initial conditions are in which stochastic viability kernel for the different RCP scenario. Furthermore, we investigate what the influence of certain parameters is on the stochastic viability kernels. Secondly, the point of no return under the different RCP scenarios is calculated. Again, for some parameters sensitivity tests are done to see how they affect the point of no return. Finally, we search for the optimal mitigation scenario using the fixed en flexible strategy. We have calculated the results for an energy balance model with $\alpha_1 = 0.2$ (tipping model) and $\alpha_1 = 0.45$ (smooth model).

4.1 Stochastic viability kernels

To create stochastic viability kernels, we need to consider $p(x,t)$ under a certain CO_2eq forcing for different initial conditions of the CO_2eq concentration and $p(x,0)$. Suppose the climate system will be forced by a certain RCP scenario from 2030 till 2200. But, the initial CO_2eq concentration in 2030, indicated by C_0, is still unknown. To have a RCP scenario for every C_0, the original RCP scenario from Fig. 3 is adjusted such that its time development remains the same, but it has C_0 as CO_2eq concentration in 2030. However, C_0 is not the only initial condition of the climate system. The PDF of the GMST $p(x,t=0)$ ($t=0$ refers to the year 2030) is also an initial condition. This will be a PDF with a set variance and a varying expectation value T_0. Subsequently, if we define viable region V, for each initial condition, consisting a of C_0 and T_0, one could calculate in which stochastic viability kernel it is located.

In Fig. 7, the stochastic viability kernels are plotted for the energy balance model forced by the RCP4.5 scenario and a viable region V defined by $T \leq 293$ K. The results for the tipping and smooth model are plotted in Fig. 7a and 7b, respectively. The colors indicate for each combination of T_0 and C_0 in which stochastic viability kernel it is located. For example, consider the tipping model and an initial condition of $T_0 = 288$ K and $C_0 = 400$ ppmv. This initial condition is in $V_{0.90}$. Since only V_β's with $\beta \in \{0.99, 0.90, 0.80, 0.70, 0.60, 0.50\}$ are considered in Fig. 7, we can conclude that this initial condition could also be in, for example, $V_{0.95}$. Furthermore, the white area suggests that these initial conditions are in a stochastic viability kernel V_β with $\beta < 0.5$.

In this subsection we first investigate the difference in stochastic viability kernels for a system forced by the RCP2.6, RCP4.5 and RCP6.0 scenario as well as how they differ for the tipping and smooth model. Subsequently, we show the effect of a changing variance of the noise and viable region on the stochastic viability kernels. We will compare these results with a reference situation, which is given in Table 2. Also, this table shows the combination of parameters that will be considered. Note that the plots can be found in the Appendix, since they are quite big.

TABLE 2: Situations that will be considered. The reference situation is bold and for the other situations, the value that differs from the reference situation is colored red.

Scenario	Variance of noise (K^2)	Viability region (K)
RCP4.5	$\boldsymbol{\sigma_s^2}$	**T $\leq$ 293**
RCP2.6	σ_s^2	T $\leq$ 293
RCP6.0	σ_s^2	T $\leq$ 293
RCP4.5	$0.5\sigma_s^2$	T $\leq$ 293
RCP4.5	$2\sigma_s^2$	T $\leq$ 293
RCP4.5	σ_s^2	T $\leq$ 291
RCP4.5	σ_s^2	T $\leq$ 295

4.1.1 RCP scenarios

In Fig. A1, the stochastic viability kernels for an energy balance model forced by RCP4.5, RCP2.6 and RCP6.0 are plotted. The left and right plots are respectively made for the tipping and smooth model. Interestingly, for both models, the plot for RCP6.0 is empty. From this we can conclude that when the energy balance model is forced with the RCP6.0 scenario, each combination of T_0 and C_0 is in a V_β with $\beta < 0.5$.

Also remarkable is the difference in stochastic viability kernels between RCP2.6 and RCP4.5. For example, consider the tipping model and the initial condition given by $T_0 = 288$ K and $C_0 = 470$ ppmv. For RCP2.6, this initial conditions is in $V_{0.99}$. This means that for each year until 2200 the GMST has at least 0.99 chance to be in the viable region. However, this is less than 0.5 for RCP4.5. This is a significant difference.

Besides, under the RCP4.5 and RCP2.6 forcing, the stochastic viability kernels $V_{0.99}$ and $V_{0.90}$ are approximately the same for the tipping and smooth model. This is because both models behave the same far from the unstable branch of the tipping model. Far from this branch, the variance of the PDF is only determined by the variance of the noise. When reaching CO_2eq levels corresponding to an equilibrium GMST close to the lower tipping point, a part of the PDF of the tipping model will "leak" away to the warmer equilibrium, which is not the case for the smooth model.

4.1.2 Variance of noise

We have investigated what the influence of different values of the variance of the noise is on the stochastic viability kernels. Fig. A2 shows the stochastic viability kernels for a variance with a value of σ_s^2, $0.5\sigma_s^2$ and $2\sigma_s^2$. When the variance of the noise is $0.5\sigma_s^2$, $V_{0.99}$ becomes significantly larger compared to the reference situation for both

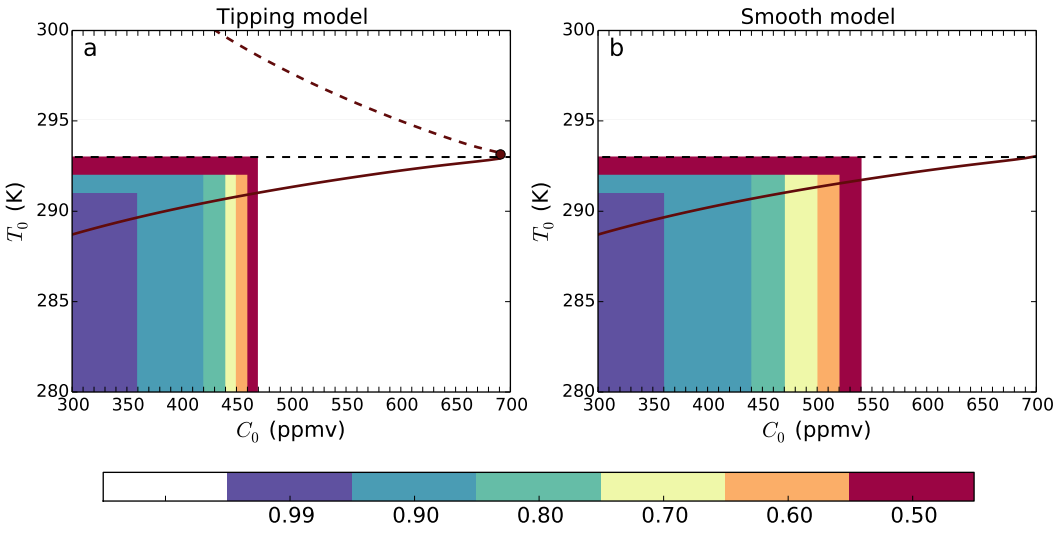

FIG. 7: The stochastic viability kernels for the tipping and smooth model forced by the RCP4.5 scenario. The viable region is defined as $T \leq 293K$ and is indicated by the black dashed line. This plots shows, for each combination of T_0 and C_0, in which stochastic viability kernel it is located. The numbers in the colorbar stand for the β in V_β. For convenience, the bifurcation diagram of the deterministic model is also depicted. This describes roughly the movement of the expected value of the PDF when the CO_2eq concentration is changing.

models. This can be clarified by a decreasing variance of the PDF of the GMST, once the variance of the noise decreases. Therefore, the expected value of the GMST, and thus the CO_2eq concentration, can become higher before the PDF of the GMST has less than 0.99 chance to be in the viable region. Other differences between the reference and $0.5\sigma_s^2$ situation are relatively small. In contrast, if a variance of $2\sigma_s^2$ is chosen, not a single initial condition will be in $V_{0.99}$. This shows how important it is to model the variance of the noise correctly.

4.1.3 *Viable region*

We consider a couple of differently defined viable regions and check what the influence is on the stochastic viability kernels. Fig. A3 consists of stochastic viability kernels for the tipping and smooth model with a viable region set by $T \leq 291$ K, $T \leq 293$ K and $T \leq 295$ K. Noteworthy is that for both models, the stochastic viability kernels are exactly the same when $T \leq 291$ K. This can be clarified by the position of the viable region relative to the tipping point. Since the intersection of the lower stable branch of tipping model and the boundary of the viable region is far from the tipping point, the dynamics of either model are identical.

When comparing the reference situation with the situation where the viable region is defined by temperatures lower or equal than 295 K, we hardly see differences in the case of the tipping model. For the smooth model, however, these differences are more remarkable. $V_{0.99}$ is a lot greater for the situation where viable region is defined as $T \leq 295$ K. The absence of the tipping point in the smooth model is the explanation. The CO_2eq concentration can be a lot higher before the PDF of the GMST has less than 0.99 in the viable region compared to the reference situation.

4.2 *Point of no return*

We will investigate whether there is a point of no return when the energy balance model is forced by the four different RCP scenarios. To do this, a tolerance probability of $\beta_T = 0.9$ and a tolerance time of $T_T = 20$ years is used. We add these two values to the reference situation. Furthermore, we investigate what the influence of a different tolerance time or tolerance probability is on the point of no return.

The points of no return for a system forced with RCP4.5, RCP6.0 and RCP8.5 are shown in Fig. 8 for both the tipping and smooth model. An important result is that the more extreme the RCP scenario, the earlier the point of no return. This can be explained by the fact that when the CO_2eq concentration is rising faster, the GMST will get non viable earlier. Consequently, the point of no return will be earlier, since the GMST is only allowed to be non viable for at most T_T years. Besides, for a system forced with RCP2.6, there is no point of no return for

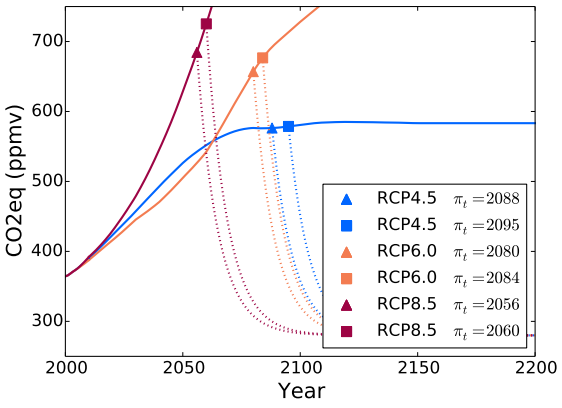

FIG. 8: The point of no return for a system forced with different RCP scenarios. We have used $\beta_T = 0.9$ and $T_T = 20$ years. The triangles indicate the point of no return for the tipping model and the squares for the smooth model. The dotted line is the most extreme scenario of F; an exponential decay to 280 ppmv with an e-folding time of 9 years. Note that for both the tipping and smooth model there is no point of no return when the system is forced with the RCP2.6 scenario.

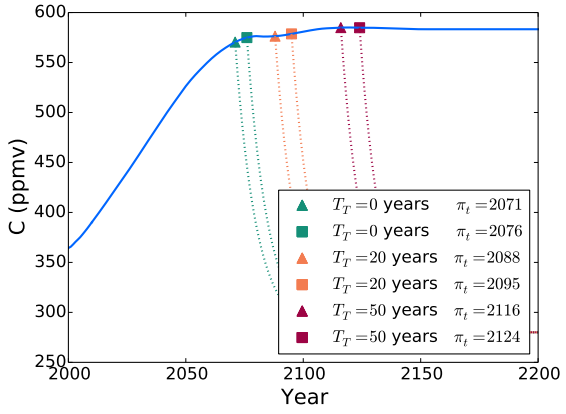

FIG. 9: The point of no return for different tolerance times. A tolerance probability of $\beta_T = 0.9$ is used. The rest is as in Fig. 8.

both the tipping and smooth model. The reason for this is that the CO_2eq concentration will remain low throughout the whole period and consequently the GMST will stay viable.

Furthermore, the π_t of the tipping model is for each scenario earlier than π_t of the smooth model. This can be clarified by the fact that the PDF of the GMST in the tipping model will leave the viable region at a lower CO_2eq concentration because of the unstable branch.

4.2.1 *Tolerance time*

According to IPCC, the CO_2eq concentration in 2030 in the RCP4.5 scenario will be 457 ppmv. From Fig. A1, it can be seen that this concentration is in $V_{0.60}$ for the tipping model and in $V_{0.80}$ for the smooth model when the GMST in 2030 is below 292 K. Since $\beta_T = 0.9$, we claim that, at least when $T_T = 0$ years, there exists a point of no return for both models.

In Fig. 9, π_t is plotted for a tolerance time of 0, 20 and 50 years for both the tipping and smooth model. For each tolerance time, there exists a point of no return. Clearly, the point of no return will be later as the tolerance time increases. Consider the difference in point of no return for a tolerance time of 20 and 50 years for the tipping model. This difference is 28 years, which is close to the difference in tolerance time (30 years). These numbers are nearly the same, since between these points of no return, the CO_2eq concentration is almost constant.

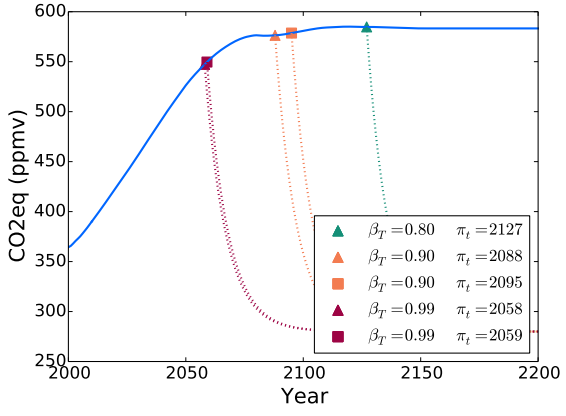

FIG. 10: The point of no return for different tolerance probabilities. A tolerance time of $T_T = 20$ years is used. Note that there does not exist a point no return for the smooth model when $\beta_T = 0.8$. The rest is as in Fig. 8.

4.2.2 *Tolerance probability*

The influence of the tolerance probability on the point of no return is shown in Fig. 10. Again, the differences between tipping and smooth model are relatively small. However, for the smooth model there does not exist a point of no return for a tolerance probability of 0.80. We could have already seen this from Fig. A1, since a CO_2eq concentration of 457 ppmv in 2030 is in $V_{0.80}$.

4.3 *Optimal mitigation scenario*

We will calculate the optimal mitigation scenario for the tipping and smooth model using the fixed and flexible strategy. To calculate this, we use the reference tolerance probability and time of $\beta_T = 0.9$ and $T_T = 20$ years. We force the system with RCP4.5 and the viable region is defined as $T \leq 293$ K. Furthermore, we choose $\Delta t = 4$ years and $\zeta = 75000$ and $C_{ref} = 500$ ppmv in the cost function. These values are somewhat arbitrary chosen, but remember that the goal is to show the concept rather than having the most realistic output.

4.3.1 *Fixed strategy*

In Fig. 11, k versus the total costs are plotted for the tipping and smooth model. The optimal mitigation scenario for the tipping and smooth model are given by $k = 50.6$ years and $k = 160.8$ years, respectively. This means that the optimal mitigation scenario for the tipping model is more extreme than the one for the smooth model. Also, the costs associated with the stringency of the mitigation and extreme weather events are plotted in Fig. 11. This reveals that the costs associated with extreme weather events are for a given k lower for the smooth model than the tipping model. These costs are directly related to the amount of years that the GMST has been non viable. Therefore, this difference can be clarified by the fact that the PDF of the tipping model will be non viable earlier because of the unstable branch.

Besides, for small k the costs associated with mitigation are lot higher for the smooth model than the tipping model. This can be explained with Eq. 15. For a given mitigation scenario, $t_e - t_c$ does not necessarily have to be same for the smooth and the tipping model, since the models are not the same. It turns out that for small k, $t_e - t_c$ is smaller for the smooth model than for the tipping model. Consequently, the calculated surface for a given scenario will be smaller for the smooth model and therefore the costs higher. However, for both models, the costs associated with the stringency of the mitigation must be the same, which is not the case. Therefore, the cost function given in Eq. 15 can only be used to find the optimal mitigation scenario for both model separately; we can not compare the costs of the optimal mitigation scenarios of both models.

Finally, the wiggles than can be seen in Fig. 11 are caused by the numerical calculations. We have used a time step of 1 month and thus some mitigation scenarios could have a similar value for $t_e - t_b$. We have not considered a smaller time step, since this would increase the computing time significantly.

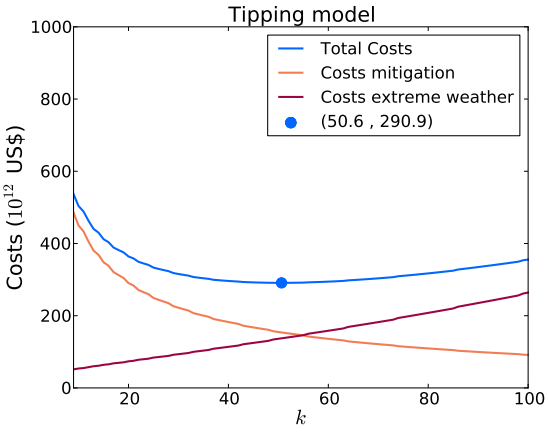

(a)

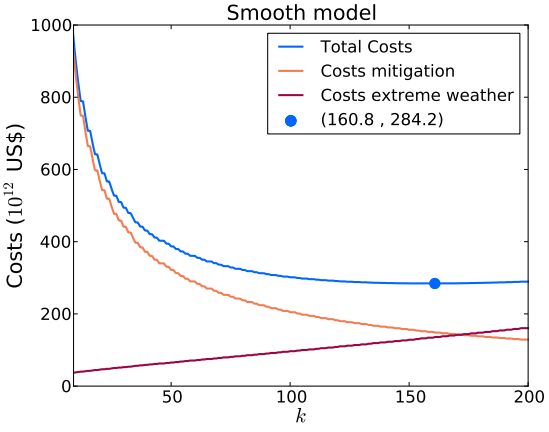

(b)

FIG. 11: The e-folding time of the exponential decay versus the costs for the (a) tipping model and (b) smooth model. The orange and red line indicate the costs associated with stringency of mitigation and extreme weather events, respectively. The optimal mitigation scenario is given by the blue dot and the associated k and costs are given in the legend. Note the difference in horizontal scale for both plots.

4.3.2 *Flexible strategy*

To calculate the optimal mitigation scenario using the flexible strategy, we use the formula in Eq. 14. In this formula, we use $E^*[X_t] = 292$ as the reference expectation value. This is approximately the expectation value of the GMST just before getting non viable. The considered linear relations between k and $E[X_t]$ are depicted in Fig. 12 by the gray area. For each mitigation scenario in F_{flex}, which is associated with a value of γ, the costs are

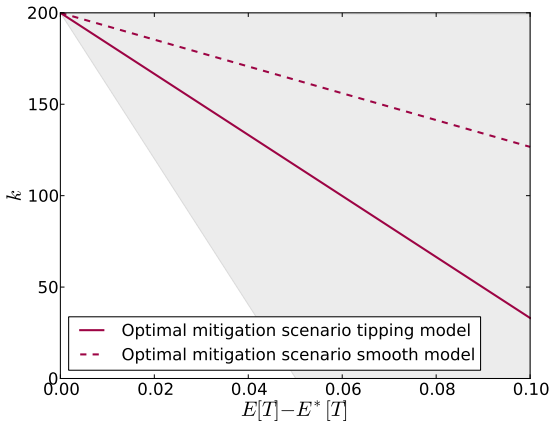

FIG. 12: The considered linear relations between Kc and $E[X_t]-E^*[X_t]$ represented by the colored area. The bold and dashed blue line are the linear relations for the optimal mitigation scenario for respectively bifurcation 1 and 2.

calculated and shown in Fig. 13. The optimal mitigation scenario for the tipping and smooth model are given by a scenario made with $\gamma = 1669.3$ and $\gamma = 773.2$, respectively.

When comparing the costs of the optimal mitigation scenario using the fixed and flexible strategy, we see that for the tipping model the fixed strategy is cheaper and for the smooth model the flexible strategy.

5 PLASIM

The next step in this study is calculating the point of no return and optimal mitigation scenario with a more realistic climate model. To do this, we use data which is generated with PLASIM. This is a simplified General Circulation Model developed by the University of Hamburg. We used the exact same data as Ragone et al. (2014), except that in this study the seasonal cycle is not removed. This results in a long-term increase of the GMST of 5 °C instead of 8 °C under a scenario where the CO_2 concentration doubles. For further specifications of PLASIM and how the used data is generated, see Ragone et al. (2014).

To find the point of no return and optimal mitigation scenario, one should be able to calculate the time evolution of the PDF of the GMST for an arbitrary CO_2eq forcing. In order to obtain this, linear response theory will be used. We will construct the first order Green function of the expectation value and variance of the GMST from the data generated with PLASIM.

We have access to two ensembles for the GMST, each of 200 experiments, made with two different CO_2 forcing profiles (all other GHGs are kept constant). For both forcing profiles, the start CO_2 concentration is set to a value

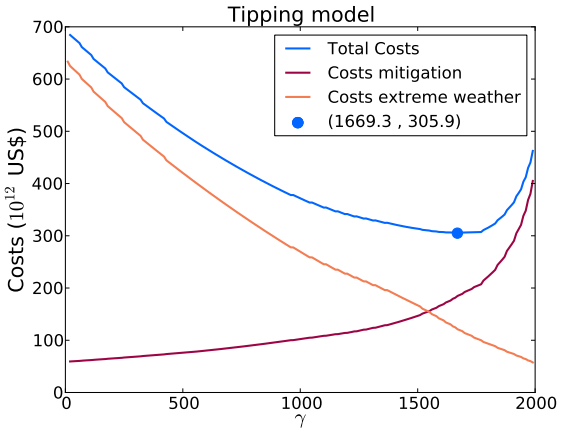

(a)

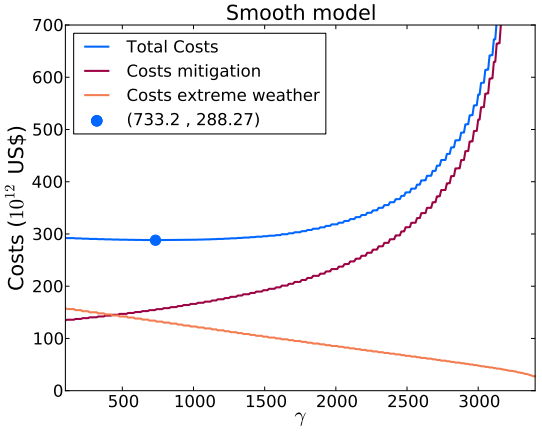

(b)

FIG. 13: γ versus the costs. The rest is as in Fig. 11

of 360 ppmv, which is representative for CO_2 concentration in 2000. During the first set of experiments, the CO_2 concentration is instantaneously doubled to 720 ppmv and kept constant afterwards. During the second set of experiments, the CO_2 concentration increases each year with 1 % until a concentration of 720 ppmv is reached. This will take approximately 70 years and afterwards the concentration is fixed. The total length of the simulations is 200 years. Furthermore, the forcing in Eq. 6 is the logarithm of the CO_2 concentration, since the radiative forcing scales approximately logarithmically with the CO_2 concentration.

In order to get the PDF of the GMST under any CO_2eq forcing, we made the assumption that at each point in time the PDF of the GMST is normally distributed. To check whether this is a good assumption, a Pearson's chi-square test has been done on the available data. At each point in

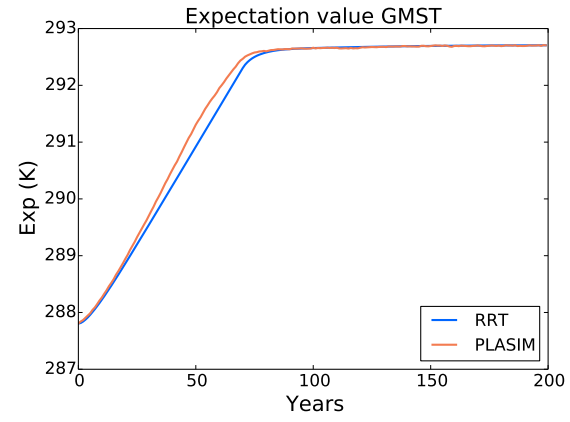

(a)

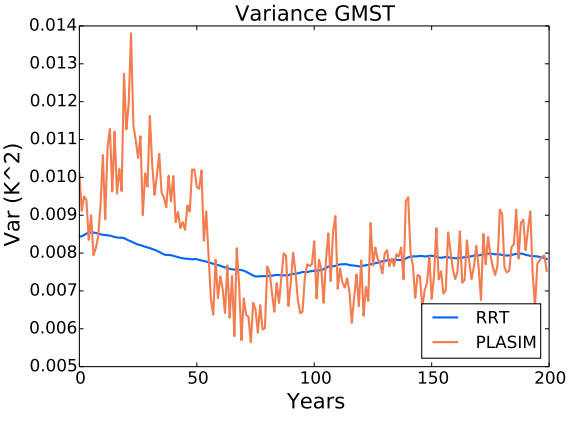

(b)

FIG. 14: (a) The expectation value and (b) variance of the GMST generated by PLASIM (orange) and made with RRT (blue).

time a PDF of the GMST has been made of the 200 ensemble members and subsequently a Pearson's chi-square test has been done. The result of this test gives the chance that 200 numbers selected from a normal distribution have the same "spread". If this chance is above 0.05, the assumption about the normal distribution is good. We found that for each point in time the result of the chi-square of the PDF of GMST was higher than 0.05. Therefore, the assumption that the PDF of the GMST is normally distributed is good.

The Green functions for the expectation value and variance have been calculated with the instantaneously doubling CO_2 profile and the associated ensemble. From the ensemble, at each point in time the expecation value and variance are calculated such that we get the temporal evolution of these two variables. Subsequently, we have found the Green functions with Eq. 7. To check whether these Green functions perform well, we compare the temporal evolution of the expectation value and variance of the GMST under the 1 % forcing calculated with Eq. 6 with those directly generated with PLASIM. The result is shown in Fig. 14.

The expectation value made with RRT is almost identical to the one directly generated by PLASIM. However, the Green function of the variance performs a lot worse. The variance of the ensemble generated by PLASIM is a lot noisier than the one made with RRT. A reason for this could be that RRT does not work well on noisy data. We have also tried to use a running mean of the variance to reduce the noisiness and checked whether that Green function performed better. However, this was not the case. Despite the fact that the Green function of the variance does not perform perfectly, we will still use it to calculate the variance of the GMST, since it predicts the variance in the right order of magnitude.

5.1 Mitigation scenarios

In this second stage of this research, the considered mitigation scenarios in F are also exponentially decaying scenarios. However, all the scenarios in F decay to different stabilisation levels, varying between 400 and 550 ppmv. We assume that stabilisation happens within 100 years, which corresponds to an e-folding time of 25 years. This is according to Edenhofer et al. (2010) a reasonable assumption. Symbolically, the mitigation scenarios in F are given by

$$f_{C_{st}}(t) = \left(\mathrm{CO_2eq}|_{t_{st}} - C_{st}\right) \exp\left(-\frac{t-t_{st}}{25}\right) + C_{st}. \quad (16)$$

In this equation is C_{st} the stabilisation level, t_{st} the time at which the mitigation scenario is applied and $\mathrm{CO_2eq}|_{t_{st}}$ the associated CO_2eq concentration. The most extreme mitigation scenario in F is the one that stabilises at a CO_2eq concentration of 400 ppmv. The collection F_{fix}, which is the collection used to find the optimal mitigation scenario using the fixed strategy, consists of the scenarios of F with $t_{st} = t_c$.

To find the optimal mitigation scenario using the flexible strategy, we need to create the collection F_{flex}. The flexible strategy used in PLASIM is different from the flexible strategy used in the energy balance model. Instead of every 5 years, the mitigation scenario can now only be re-chosen in 2070. However, in 2070 there are no limitation about how to choose a scenario from F; every scenario can be chosen. In order to make it less computational heavy to find optimal mitigation scenario, only scenarios in F that stabilises at a CO_2eq level of $C_{st} = 400, 405, 410, .. , 550$ ppmv can be chosen at t_c and in 2070.

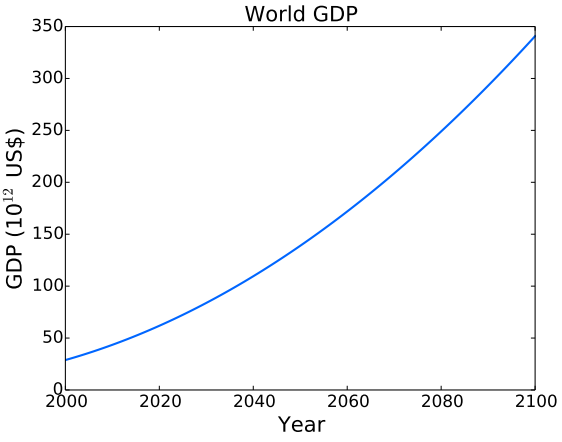

(a)

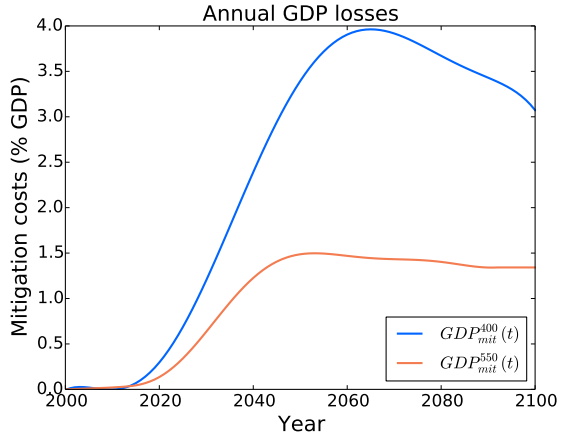

(b)

FIG. 15: (a) The expected rise of GDP expressed in US dollars and (b) the annual economic costs of stabilising after 100 years at CO_2eq levels of 400 ppmv and 550 ppmv. Both figures are from Edenhofer et al. (2010) and made with the POLES model. Note that to calculate the annual costs of stabilising at an other CO_2eq level, for each year we linearly interpolate the costs.

5.2 Cost function

Each mitigation scenario has its own economic costs. The costs associated with the stringency of mitigation will be determined using the output of the POLES model. This is a energy-environment-economy model and used by Edenhofer et al. (2010) to calculate the economics of low CO_2eq stabilisation. The annual costs of stabilising at CO_2eq levels of 400 ppmv and 550 ppmv are shown in Fig. 15(b) (Edenhofer et al. 2010). The costs are expressed in percentage of the global gross domestic product (GDP), which is a monetary measure of the value of all final goods and services produced in a year. The cost for stabilising at 400 ppmv are a lot higher than for stabilising at 500 ppmv. This is because such a low stabilisation can only be reached when new technologies, like energy made out of biomass and carbon storage, are used on a large scale. Furthermore, Fig. 15(a) reveals how the POLES model expects the GDP to increase till 2100.

In order to calculate the economic costs of a mitigation scenarios that stabilise at a certain CO_2eq levels, the following assumptions are made.

- To calculate the annual costs of a mitigation scenario that stabilises at an other CO_2eq level than 400 or 550 ppmv, for each year we linearly interpolate the costs. The annual GDP loss associated with a scenario that stabilises at C_{st} is given by the function $GDP^{C_{st}}_{mit}(t)$
- We do not take into account the value of the maximum in CO_2eq concentration. For example, the costs associated with mitigation for a scenario that stabilises at a value of 400 ppmv are the same for a scenario that has a CO_2eq concentration at t_c of 600 and 700 ppmv. We will accept this, since the other option is that for any CO_2eq concentration at t_c, we need to consider what the possible mitigation scenarios are. This is beyond the scope of this study.
- We will only charge costs for mitigation between $t = t_c$ and $t = 2100$

Consequently, the costs associated with the stringency of mitigation for a monotonically decreasing mitigation scenario are given by the first part of Eq. 17.

$$\Psi\big(f(t)\big) = \underbrace{\sum_{t=t_c}^{2100} GDP(t) * GDP^{C_{st}}_{mit}(t)/100}_{1} + \underbrace{\sum_{t=t_b}^{t_e} GDP(t) * GDP_{ewe}/100}_{2} \tag{17}$$

Stern (2007) estimated the annual costs associated with damage of extreme weather events, when the temperature reaches a value of 2 °C above the preindustrial temperature, at 0.5-1.0 % of the GDP. In this study we will charge 1.0 % GDP (GDP_{ewe}) for every year the GMST is not viable. Note that the viable region is defined by GMSTs lower than a temperature of 2 °C above preindustrial GMST. Furthermore, when the temperature is viable, no costs will be charged. Symbolically, this part of the cost function is given by part two of Eq. 17.

Finally, the optimal mitigation scenario, for the fixed and flexible strategy, can be found by minimising the cost function Ψ under the restriction that the climate must be viable in 2100.

6 Results PLASIM

In this section, we present the results calculated with the data of PLASIM in combination with RRT. Firstly, we determine the point of no return for the different RCP scenarios. To do this, we used the second definition of the point of no return, which requires that the GMST must be viable in 2100, and a tolerance probability of $\beta_T = 0.90$. Furthermore, the viable region is set at $T \leq 287.15$ K , which corresponds to temperatures lower than 2 K above the preindustrial GMST. The boundary of this viable region can be considered as a threshold of dangerous human interference and for avoiding the worst impacts of climate change (Mann 2009). Secondly, we show what the influence of a different β_T is on the point of no return. Thereafter, the optimal mitigation scenario is calculated using the fixed and flexible strategy with $\Delta t = 4$ years. Finally, we show what the influence is of an increasing Δt on the minimal costs for the fixed strategy.

6.1 Point of no return

We have found a point of no return for all the RCP scenarios except the RCP2.6 scenario. They are plotted in Fig. 16. The solid lines represent the RCP scenarios and the dashed lines present the most extreme scenario from F. The point of no return under the RCP8.5 forcing is 12 years earlier than under the RCP4.5 and RCP6.0 forcing, since the CO_2eq concentration increases much faster for the RCP8.5 scenario. However, the mitigation scenario after the point of no return, represented by the dashed line, is for all RCP scenarios the same. This is because the definition of the point of no return states that the GMST must be viable in 2100. The scenario that is plotted is the ultimate scenario that guarantees this. Moreover, this indicates that, if the mitigation scenario plotted in Fig. 16 is extended for years smaller than 2053, for each CO_2 scenario the associated point of no return is given by the intersection of that CO_2eq scenario and the extended mitigation scenario. This is because we claim that an exponential decay to 400 ppmv within 100 years is always possible, no matter the CO_2eq concentration at t_c. However, when this concentration becomes to high, this mitigation scenario is not realistic anymore.

6.1.1 Tolerance probability

The influence of the tolerance probability on the point of no return for the RCP4.5 scenario is plotted in Fig. 17. We consider a tolerance probability of 0.8, 0.9 and 0.99. When the tolerance probability is higher, it takes longer before the GMST will be viable again and thus the point of no return will be earlier. However, the differences are very small, since the ultimate scenarios that guarantee viability in 2100 for the different tolerance probabilities are very close to each other.

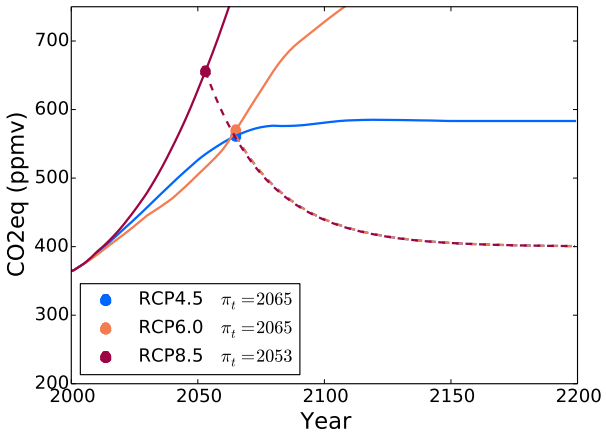

FIG. 16: The points of no return for the RCP4.5, RCP6.0 and RCP8.5 scenarios for a tolerance probability of $\beta_T = 0.9$. There is no point of no return for the RCP2.6 scenario. The solid lines represent the RCP scenarios and the dashed line the most extreme scenario from F. Note that these dashed lines coincide.

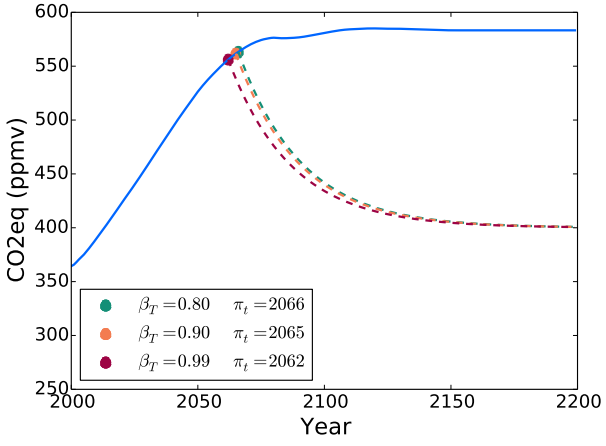

FIG. 17: The point of no return for RCP4.5 for different tolerance probabilities. The solid and dashed lines are as in Fig. 16

6.2 Optimal mitigation scenario

We find that, under a forcing of the RCP4.5 scenario, the first year of non viability is 2033. Since we have set $\Delta t = 4$ years, the year we start mitigating is 2037. From this time, we mitigate with a scenario from F_{fix} or F_{flex}. In Fig. 18, the costs are plotted for the different mitigation

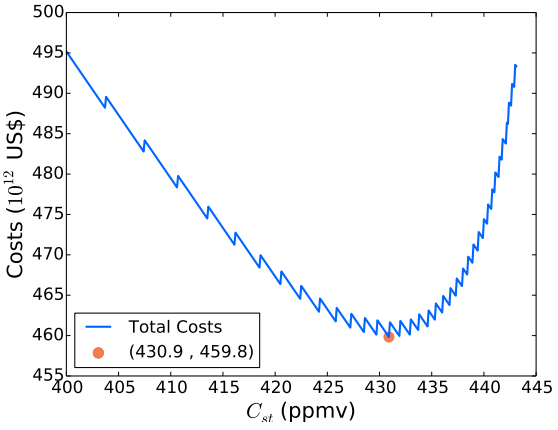

FIG. 18: The costs for the different mitigation scenarios. On the horizontal axis is the stabilisation CO_2eq level of the scenarios in F_{fix}. The optimal mitigation scenario is shown by the orange dot. The associated costs can be found in the legend.

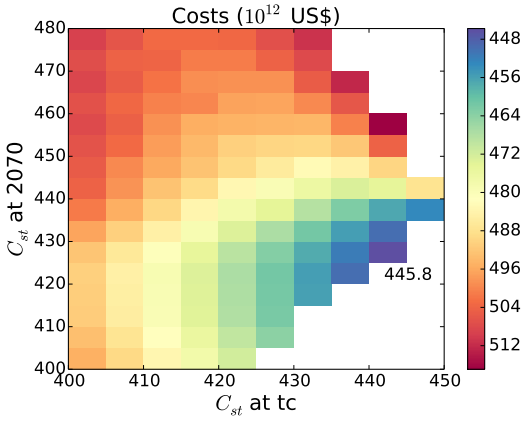

FIG. 19: The costs for the different mitigation scenarios in F_{flex}. On the horizontal axis is the stabilisation concentration of the scenario chosen at t_c and on the vertical axis the stabilisation concentration of the scenario chosen at 2070.

scenarios from F_{fix}. Stabilisation concentrations of 444 ppmv and higher are not considered, since these scenarios do not guarantee that the GMST is viable in 2100. The optimal mitigation scenario is a scenario that stabilises at a CO_2eq concentration of 430.9 ppmv.

The wiggles in Fig. 18 can be explained by the fact that for some scenarios the amount of years of non viability are the same. However, the period of the wiggles gets smaller as the stabilisation CO_2eq concentrations increases. To explain this, we assume that the moment of getting viable again (t_e) corresponds with a certain reference CO_2eq concentration. During low stabilisation, the decrease in CO_2eq concentration is steep and there is not much time between the intersection of two consecutive mitigation scenarios with this reference concentration. However, when the stabilisation concentration is higher, the decrease in CO_2eq concentration will be less steep, and there is more time between the intersection of two consecutive scenarios and the reference concentration.

In Fig. 19, the costs are given for the different scenarios using the flexible strategy. The white area indicates scenarios that are not viable in 2100. The optimal mitigation scenario is given by a scenario that stabilises around 440 ppmv within 100 years at t_c and around 425 ppmv at 2070. The associated costs of the optimal mitigation scenario using the flexible strategy are lower than using the fixed strategy. Moreover, we only considered a few of the possible flexible scenarios, so the economic costs could even be lower.

6.3 *Increasing* Δt

Fig. 20 shows how the costs of the optimal mitigation scenario using the fixed strategy change when Δt increases. The previous results are made with $\Delta t = 4$ years and $\Delta t = 32$ years corresponds with the point of no return. From Fig. 18 we have seen that for $\Delta t = 4$ years, the minimal costs are $459.8 * 10^{12}$ US dollars. However, Fig. 20 shows that the costs of the optimal mitigation are above $460 * 10^{12}$ US dollars. This is because the costs in Fig. 18 are calculated for stabilisation levels of $C_{st} = 400, 400.1, 400.2, .., 550$ ppmv and in Fig. 20 only for $C_{st} = 400, 401, 402, .., 550$ ppmv.

Fig. 20 reveals that there is a Δt that maximises the costs of the optimal mitigation scenario. This can be clarified by a respectively increase and decrease of the costs associated with extreme weather and stringency of mitigation when Δt increases. When Δt increases, the time between t_b and t_e will increase and thus the costs associated with extreme weather events increases. Also, when Δt increases, the optimal mitigation scenario may be steeper and thus more expensive. However, since the time between t_c and 2100 will decrease as well, the eventual costs associated with the stringency of mitigation decrease once Δt increases.

7 Discussion

In this study we have defined the point of no return in climate change more precisely, using stochastic viability theory in which we determine a tolerance probability and a viable region. We defined the point of no return as a point in time by which we need to reduce the global GHG concentration to guarantee viability of the GMST in 2100. We now place our results in a broader context and discuss the

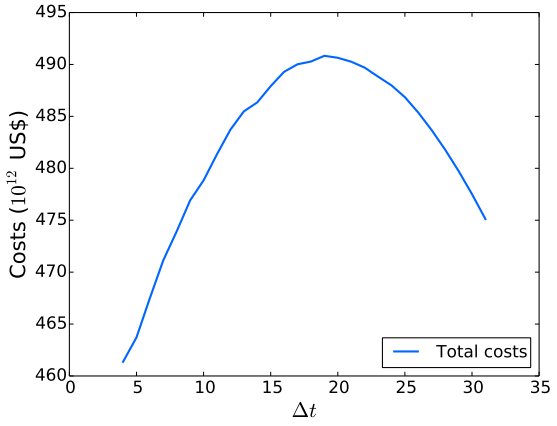

FIG. 20: The costs of the optimal mitigation scenario using the fixed strategy for different Δt. The point of no return corresponds with $\Delta t = 32$ years.

applications of the defined point of no return. We furthermore discuss how the presented model could be improved for future studies.

7.1 Point of no return; implications for decision making

We defined the point of no return is such a manner that for each arbitrary CO_2eq scenario the point of no return can be determined. Using the definition that guarantees that the GMST is below the 2 °C level in 2100 (note that the 2 °C level refers to a GMST of 2 °C higher than the preindustrial GMST), we found that the point of no return for the RCP4.5 and RCP6.0 scenario is in 2065. In this definition, however, we allow the GMST to exceed the 2 °C level before 2100. Nevertheless, if the aim is to stay below this 2 °C level, as argued in 2009 Copenhagen Accord, we need to take action much earlier. Specifically, when using a tolerance probability of $\beta_T = 0.9$, we found that the first year of non viability under the RCP4.5 scenario in PLASIM is 2033. This means that in 2033, the chance that the GMST is above the 2 °C level is greater than 0.1. Consequently, we can conclude that reduction of CO_2eq concentration must occur before 2033 to guarantee that the GMST stays below the 2 °C level.

Rogelj et al. (2013) found that if the CO_2eq emission in 2020 is between 40 and 47 Gt, the GMST will stay below the 2 °C level. According to IPCC, the emission in 2020 associated with the RCP4.5 is 48 Gt and thus according to Rogelj et al. (2013) the temperature will exceed the 2 °C level. However, as indicated in this study there is still a possibility to stay below the 2 °C level before 2033 and hence there is 13 years more time to reduce anthropogenic GHGs emissions. Nonetheless, we suggest to reduce the GHGs concentration sooner rather than later in order to prevent from disastrous global climate impacts and to minimise the economic costs.

We used a viability region that was defined as GMSTs lower than the 2 °C level. The 2 °C level gained a lot of prominence in the early 1990s when a number of international scientific panels suggested that this level would prevent us from some of the worst impacts of climate change. Recently, during the 2015 Paris Climate Conference, it was decided that 1.5 °C is a significantly safer threshold against the worst impacts of a changing climate. The advantage of the newly defined point of no return, is that the viable region can easily be changed to GMSTs lower than 1.5 °C level and subsequently we can calculate the associated point of no return. In addition, Victor and Kennel (2014) stated the 2 °C level is both politically and scientifically wrongly stated. The authors proposed that there are better ways to measure how much stress humans are placing on the climate system than the increase in the GMST. In this study, we have placed the viable constraints on the GMST. However, the viable constraints can also be placed on other variables than the GMST.

These above-mentioned aspects confirm that our framework has high potential in both political and scientific field. We defined the point of no return in such a manner that for each arbitrary CO_2eq scenario the point of no return can be determined, where the point of no return is expressed in time. By contrast, previous work ((i.e. Hansen et al. 2008; Rogelj et al. 2013) defined a point of no return as an emission level in 2020 or a certain CO_2 concentration. We suggest that a point of no return in climate change that is expressed in time, is significantly more applicable during policymaking and political debates. Furthermore, the definition of the point of no return can easily be changed according to any desired political policy or scientific approach. We thus conclude that our novel approach of the point of no return in climate change is an useful decision-making tool during future debates about climate change.

7.2 Model improvements

Although our approach provides new insights into the point of no return in climate change, we recognize here is potential to further improve our approach. The assumption about the most extreme scenario from F is too simplified is this study. This is considered to be an exponential decay to 400 ppmv within 100 years. However, once the CO_2eq concentration at t_c is very high, this is an unrealistic scenario. Therefore, further research must be done to determine the most extreme mitigation scenario for each CO_2eq concentration.

We designed a cost function to find the optimal mitigation scenario in PLASIM. The costs associated with the stringency of the mitigation scenario are calculated using

the POLES model. In this model the economic costs are given for one specific CO_2eq scenario that stabilises at 400 ppmv. However, we use these costs to calculate the costs for any scenario that stabilises at 400 ppmv, no matter the CO_2eq concentration at t_c. This is a shortcoming in our cost function. This can be improved by having access to the POLES model, such that we can calculate the costs for each separate mitigation scenario.

Another shortcoming in the cost function lies in the part that calculates the costs associated with extreme weather events. We only charge costs for extreme weather events when the GMST is not viable. Also, for each year that the GMST is not viable, no matter the height of the GMST, the costs are given by the same percentage of the GDP. Furthermore, we only consider costs associated with stringency of mitigation and extreme weather events. However, there are a lot more factors that influence the economic costs, for example, sea level rise, agriculture and human health. We suggest that a more realistic cost-function could be designed after a detailed literature study to the economic impact of climate change. This is, however, a very complex study as indicated by Stern (2007) and beyond the scope of this study.

Furthermore, we have used RRT to find the point of no return and optimal mitigation scenario in PLASIM. We have used this to find the temporal evolution of the expectation value and variance of the GMST under any CO_2eq forcing. We found that RRT does a good job by finding the right expectation value of the GMST. However, the RRT does not predict the variance that well. More research must be done to see how this can be improved and on the applicability of RRT to calculate the variance of observables of a climate model.

7.3 Concluding statements

To complete this study, we sum up our main results.

- We found that, using the energy balance model, the point of no return is earlier in a model with tipping point compared to a model without tipping point.
- Using PLASIM, we found that the point of no return for the RCP4.5 and RCP6.0 scenario is 2065. This means that at this time there is no possibility for the GMST to become viable in 2100.
- The economic costs of the optimal mitigation scenario in PLASIM are lower when a flexible strategy is used compared to a fixed strategy.
- When using the fixed strategy, we conclude that the sooner we start mitigating the cheaper it is.

Acknowledgments. First of all I would like to thank Henk for supervising me during this Master project and always being enthusiastic about the topic. Also, I would like to thank Qingyi for helping me during the first part of my research. A special thank to my sister Marit for helping me to improve my writing skills and the mental support. Thank you Aleid, René, Robby and Tjebbe for the relaxed lunch breaks and helping me with any problem I encountered during this last year. Finally, I would like to thank my parents, Cor and Wilma, for the unconditional support during my studies.

References

Aubin, J.-P., 2009: *Viability theory*. Springer Science & Business Media.

Budyko, M., 1969: Effect of solar radiation variation on climate of earth.

Doyen, L., and M. De Lara, 2010: Stochastic viability and dynamic programming. *Systems & Control Letters*, **59 (10)**, 629–634.

Edenhofer, O., and Coauthors, 2010: The economics of low stabilization: model comparison of mitigation strategies and costs. *The Energy Journal*, 11–48.

Fraedrich, K., H. Jansen, E. Kirk, U. Luksch, and F. Lunkeit, 2005: The planet simulator: Towards a user friendly model. *Meteorologische Zeitschrift*, **14 (3)**, 299–304.

Hansen, J., and Coauthors, 2008: Target atmospheric co2: Where should humanity aim? *arXiv preprint arXiv:0804.1126*.

Hogg, A. M., 2008: Glacial cycles and carbon dioxide: A conceptual model. *Geophysical research letters*, **35 (1)**.

Lenton, T. M., H. Held, E. Kriegler, J. W. Hall, W. Lucht, S. Rahmstorf, and H. J. Schellnhuber, 2008: Tipping elements in the earth's climate system. *Proceedings of the National Academy of Sciences*, **105 (6)**, 1786–1793.

Mann, M. E., 2009: Defining dangerous anthropogenic interference. *Proceedings of the National Academy of Sciences*, **106 (11)**, 4065–4066.

Nordhaus, W. D., 1994: *Managing the global commons: the economics of climate change*, Vol. 31. MIT press Cambridge, MA.

Pachauri, R. K., and Coauthors, 2014a: Climate change 2014: Synthesis report. contribution of working groups i, ii and iii to the fifth assessment report of the intergovernmental panel on climate change.

Pachauri, R. K., and Coauthors, 2014b: Climate change 2014: Synthesis report. contribution of working groups i, ii and iii to the fifth assessment report of the intergovernmental panel on climate change.

Ragone, F., V. Lucarini, and F. Lunkeit, 2014: A new framework for climate sensitivity and prediction: a modelling perspective. *arXiv preprint arXiv:1403.4908*.

Rogelj, J., D. L. McCollum, B. C. O?Neill, and K. Riahi, 2013: 2020 emissions levels required to limit warming to below 2 [thinsp][deg] c. *Nature Climate Change*, **3 (4)**, 405–412.

Ruelle, D., 1998: General linear response formula in statistical mechanics, and the fluctuation-dissipation theorem far from equilibrium. *Physics Letters A*, **245 (3)**, 220–224.

Ruelle, D., 2009: A review of linear response theory for general differentiable dynamical systems. *Nonlinearity*, **22 (4)**, 855.

Sellers, W. D., 1969: A global climatic model based on the energy balance of the earth-atmosphere system. *Journal of Applied Meteorology*, **8 (3)**, 392–400.

Stern, N., 2007: *The economics of climate change: the Stern review*. cambridge University press.

Tol, R. S., 2002: Estimates of the damage costs of climate change. part 1: Benchmark estimates. *Environmental and resource Economics*, **21 (1)**, 47–73.

Victor, D. G., and C. F. Kennel, 2014: Climate policy: Ditch the 2 c warming goal. *Nature*, **514 (7520)**.

APPENDIX

Figures

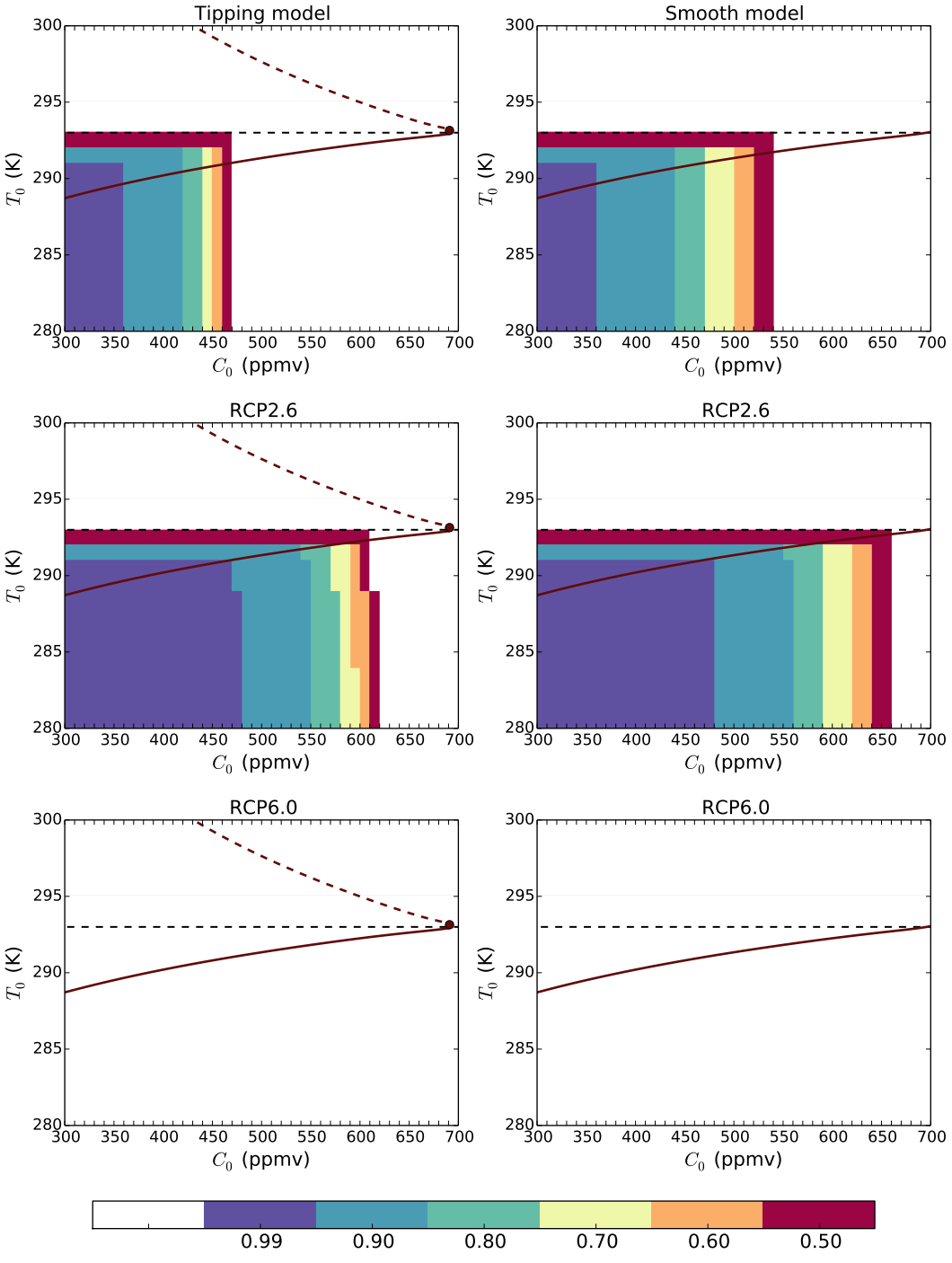

FIG. A1: Stochastic viability kernels for the energy balance model forced by RCP4.5, RCP2.6 and RCP6.0. The left and right plots are made for the tipping and smooth model respectively. The top two plots are the reference plots (see Table. 2). The numbers in the colorbar stand for β in V_β.

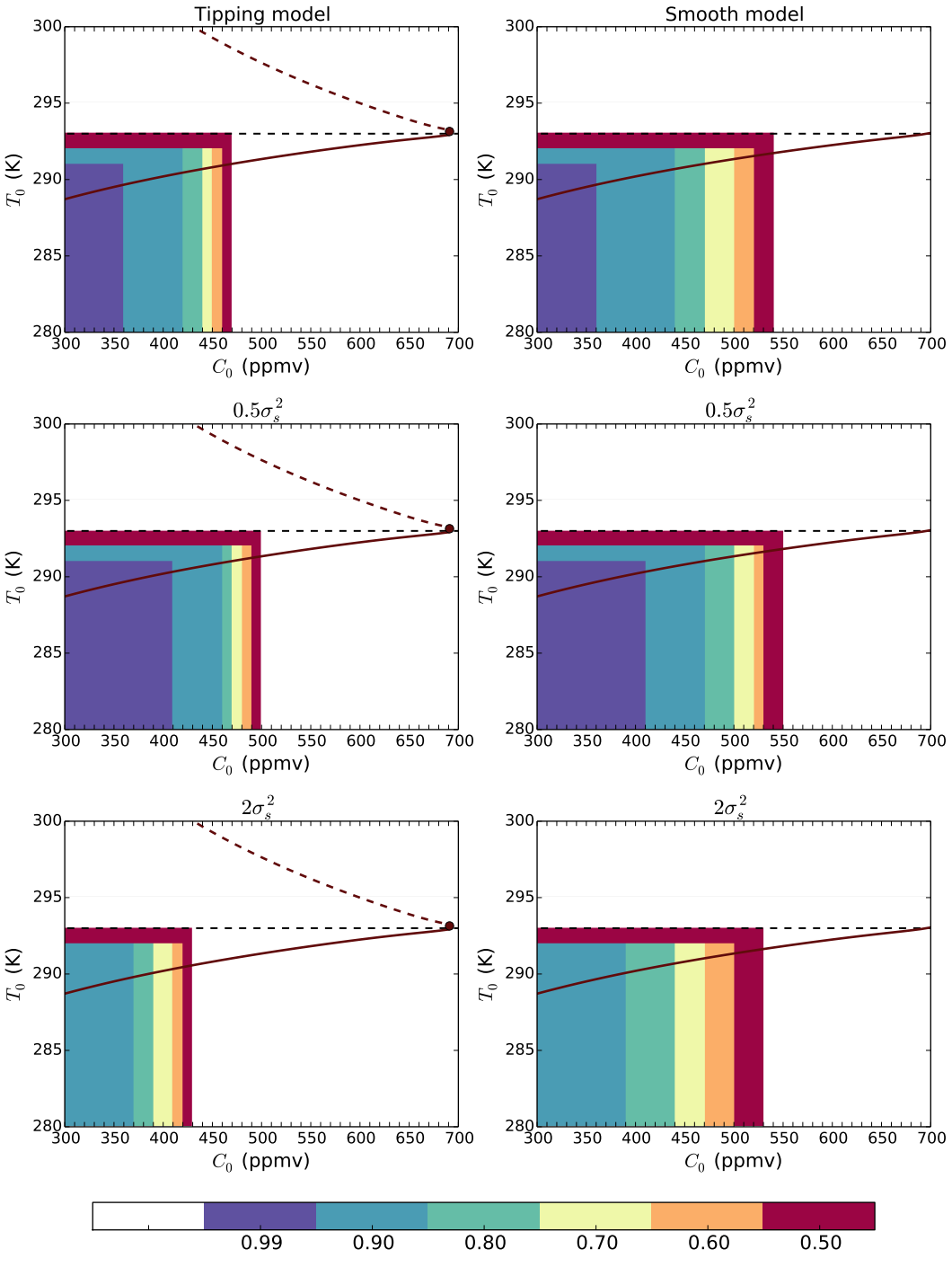

FIG. A2: Stochastic viability kernels for different values of the variance of the noise. We consider a variance of σ_s^2 (the reference situation), $0.5\sigma_s^2$ and $2\sigma_s^2$. The rest is as in Fig. A1

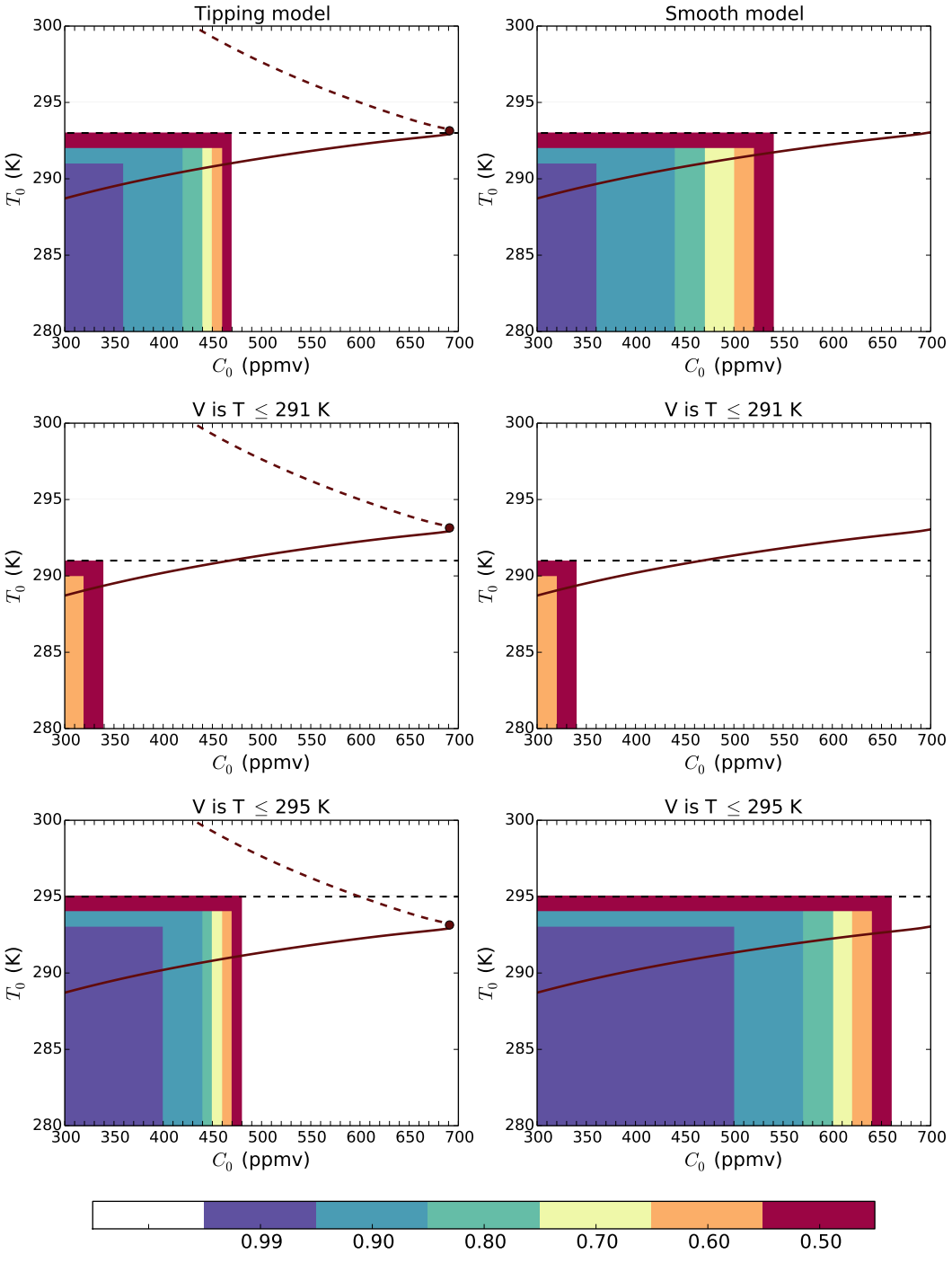

FIG. A3: Stochastic viability plot for different viable regions. Viable regions of $T \leq 291$ K, $T \leq 293$ K and $T \leq 295$ K are considered. Note that the stochastic viability kernels for $T \leq 291$ K are identical for both models. The rest is as in Fig. A1